Article to be published in "Encyclopedia of Applied Physics,"
copyright VCH Publishers, New York & Weinheim, Germany.

Spectrometers, Gamma

M. M. Lowry, C. Woody, S. Hoblit, M. Lucas, and A. M. Sandorfi,

Brookhaven National Laboratory, Upton, New York, U.S.A.

March 13, 1996

Contents

Glossary **3**

Introduction **3**

1 Energy Deposition of Gamma Rays in Materials **4**

2 Shower Development **5**

2.1 Longitudinal Development 6

2.2 Transverse Development 7

3 Calorimetry Techniques **8**

3.1 Calorimeter Types 8

3.2 Energy Measurement 10

4 Factors Affecting Gamma-ray Calorimeter Response **12**

4.1 Energy Resolution 12

4.2 Position Resolution 15

4.3 Time Resolution 16

5 Readout Devices **18**

5.1 Optical Detectors 18

5.2 Readout Electronics 19

Works Cited **20**

Further Reading **21**

Tables **22**

Figures **24**

Abstract

Gamma rays above the threshold for creation of electron-positron pairs interact with matter by initiating an electron-gamma cascade shower. This section deals with the techniques and devices for the study of such gamma rays. The relevant physical processes in cascade showers are explained, and the showers are characterized. The methods and materials used in calorimetric detectors are surveyed. The factors limiting energy, time and position resolutions are discussed.

Glossary

bremsstrahlung Gamma ray emitted by a high energy electron interacting with the electric field of a nucleus or atomic electron.

calorimeter Device that measures the total energy it absorbs.

Cherenkov radiation Photons produced by a charged particle when its velocity in the medium exceeds that of the photons in the medium.

Compton scattering Elastic scattering of a gamma ray from an atomic electron.

pair production Transformation of a gamma ray interacting with the electric field of a nucleus or atomic electron into an electron-positron pair.

photoelectric absorption Absorption of a gamma ray and emission of a previously bound electron with essentially all the energy of the gamma ray minus the binding energy of the emitted electron.

photomultiplier tube Device that generates a current pulse when struck by an optical photon via a cascade multipication of the secondary electron.

Introduction

Gamma rays are the highest energy photons in the electromagnetic spectrum. On the low energy side they overlap with the X-rays, and the interested reader is directed to that section for a discussion of the techniques appropriate for the study of gamma rays of energy less than a few MeV. Photons with energies above the threshold for creation of electron-positron pairs interact with matter by initiating a cascade shower. Sections 1 and 2 discuss the physical processes occuring within the shower and the typical characteristics of the shower. Measurements on the shower allow determination of the gamma ray properties of total energy, arrival position and time. The calorimeter detectors which perform this function are described in Sections 3, 4 and 5.

1 Energy Deposition of Gamma Rays in Materials

Gamma rays produce no detectable phenomena in free space. It is only through their interaction with matter, and specifically, the generation of charged particles, that they can be detected and studied. Fig. 1 illustrates the contribution to that interaction made by the three main interaction processes. For the experimentally important scintillation crystal, sodium iodide, it shows the components of the attenuation coefficient, $a(E_\gamma)$, the parameter describing the exponential attenuation of the number, N, of incident gamma rays as they travel through a crystal to a depth x, as a function of the gamma ray energy, E_γ,

$$N = N_0 e^{-x \cdot a(E_\gamma)}. \tag{1}$$

The dominant process at low energy (≤ 0.2 MeV) is photoelectric absorption of the gamma ray. This results in the emission of a previously bound atomic electron with essentially all the energy of the gamma ray minus the binding energy of the emitted electron. As the incident energy is raised, the next phenomenon to become important is Compton scattering. In this case, an atomic electron is again struck but the gamma ray is not absorbed. Instead the gamma ray scatters from the electron and imparts a fraction of its energy to the struck particle, depending on the angle of scattering. This process is principally important in the transition region of energy before the onset of the third interaction phenomenon.

Pair production is the dominant process by which gamma rays interact with matter in the energy regime above the threshold energy for creating electron-positron pairs ($\geq$ 1.02 MeV). The gamma ray is transformed into a pair of charged particles, an electron and its anti-particle, a positron. The process requires a virtual photon from the electromagnetic field around a nucleus or electron in order to conserve both energy and momentum. But essentially all the gamma ray energy is split between the electron and positron. The pair emerge nearly symmetrically arranged along the original gamma ray direction with a small average angle between the electron and the gamma of $\theta_e \sim m_e c^2 / E_\gamma$, where $m_e c^2$ is the rest mass energy of the electron, 0.511 MeV.

2 Shower Development

There are two main processes by which energetic electrons (and positrons) are brought to rest: 1) collisions with atomic electrons resulting in either ionization energy loss for soft collisions or division of the energy between the incident particle and the atomic electron for harder collisions, and 2) emission of a gamma ray in the electromagnetic field of a nucleus or electron, termed bremsstrahlung. (For positrons, there is the additional process of annihilation, but this mainly occurs at rest and produces two gamma rays each with half the pair creation threshold energy.) Collisional energy losses dominate at low energy but bremsstrahlung dominates at high energy. The crossover point is at a material dependent critical energy

(Bethe, Askin, 1953),

$$E_c \simeq 1600\frac{m_e c^2}{Z_{eff}}, \tag{2}$$

where $m_e c^2$ is the rest mass energy of the electron, 0.511 MeV, and Z_{eff} is an appropriately weighted average of the nuclear charge of the material constituents. It is interesting to note that the dominant high energy electron interaction, bremsstrahlung, is related by crossing symmetry to the dominant high energy photon interaction, pair production. Thus, it is not surprising that the length of material in which a high energy electron loses 1/e of its energy to radiation, the radiation length, X_0 (Tsai, 1974),

$$1/X_0 \simeq 4Z(Z+1)n\alpha r_e^2 \ln(183Z^{-1/3}), \tag{3}$$

is approximately the same as the mean distance for a high energy gamma to travel before producing a pair, λ_{pair},

$$1/\lambda_{pair} \simeq (7/9)4Z(Z+1)n\alpha r_e^2 \ln(183Z^{-1/3}), \tag{4}$$

where Z is the charge of the nucleus, $n = \rho N_a/A$ is the atomic number density, ρ is the mass density of the absorber, N_a is Avogadro's number, A is the atomic weight of the nucleus, α is the fine structure constant, 1/137, and r_e is the classical radius of the electron, 2.8×10^{-13} cm. Similarly the emission angle beween the bremsstrahlung gamma and the initial electron is characterized by the same angle, $\theta_\gamma \sim m_e c^2/E_e$, as the pair emission.

2.1 Longitudinal Development

The effect of combining these two processes, bremsstrahlung and pair production, is the creation of an electron-gamma cascade shower as shown schematically in Fig. 2. An incident gamma ray produces an electron-positron pair of particles, which then lose energy by radiating lower energy gammas, which in turn generate more pairs, and so on, until the electrons and positrons are below E_c and no longer lose significant energy by radiation. The strong forward peaking of the pair and bremsstrahlung emission means the shower tends to progress in a straight line along the initial direction. A vastly oversimplified approximation to the showering process would be that the average energy per particle is halved in each radiation length and the number of particles doubles until the average energy is reduced to the critical energy, at which point the shower terminates. Then the shower linear extent is $\sim X_0 \ln(E_\gamma/E_c)/\ln 2$ and the maximum number of particles just $\sim E_\gamma/E_c$ with approximately equal numbers of gamma rays, electrons, and positrons at each step. Finally, the integral track length of the charged particles in this simplified model is $\sim \frac{2}{3\ln 2}(E_\gamma/E_c)X_0$. More detailed calculations support these three qualitative features: the shower depth is logarithmic in incident energy, and the number of shower particles and the integral track length are both proportional to the incident energy.

2.2 Transverse Development

After the first few radiation lengths, the transverse extent of the shower is determined by the multiple scattering of the electrons and positrons. Using the Molière theory of multiple scattering (Scott, 1963), the lateral displacement of an electron with energy equal to the critical energy traveling a distance of one radiation length defines the so-called Molière radius,

$$R_M = \sqrt{\frac{4\pi}{\alpha}} m_e c^2 \frac{X_0}{E_c}, \tag{5}$$

which characterizes the shower distribution perpendicular to the shower axis. Experimentally it is found that a cylinder of radius $1R_M$ contains $\sim 90\%$ of the shower energy deposition, $2R_M \sim 97\%$ and $3R_M \sim 99\%$ (Kleinknecht, 1982).

Fig. 3 and Fig. 4 present the results of detailed simulations of such electron-gamma cascade showers in NaI with the GEANT Monte Carlo program (Brun, Carminati, 1993). Fig. 3 shows contours of the energy deposition along and transverse to the initial direction for gamma rays of 20 MeV and 20 GeV. This is the result of averaging over many such showers. As can be seen, the factor of 1000 increase in energy between the two showers produces a deeper penetration, by about ten ($\simeq \log_2(1000)$) radiation lengths ($X_0 = 2.6$ cm in NaI, Table 1). Both showers exhibit similar radial extent, approximately equal to the Molière radius ($R_M = 4.5$ cm in NaI, Table 1). Any given shower will produce a much more sparse and random energy deposition. Fig. 4 attempts to give a feeling for this by plotting the average number of 1 cm NaI cubes in which any shower energy deposition has occurred as a function of incident gamma ray energy. For the 20 MeV case, this is only 20 cubes versus the 3400 cm^3 required in Fig. 3 to contain 90% of the energy. For the 20 GeV case, the comparison is 6820 cubes versus 7000 cm^3.

3 Calorimetry Techniques

3.1 Calorimeter Types

Gamma ray detection takes place through the fundamental interactions of photons with matter described above. At high energies, the dominant process of pair production leads to electron positron pairs which undergo ionization and radiative energy loss in the detector material. The calorimetry technique makes use of the fact that this energy loss is proportional to the total energy deposited in the detector in order to measure the initial photon energy. There are in general two classes of calorimeters which are used to measure this energy. The first consists of a *totally active* detector in which all the initial energy is deposited in a material which produces an observable signal. The second is a *sampling* detector in which only a fraction of the initial energy is deposited in an active material, and the rest is deposited in a passive material and is not observed.

Totally active detectors usually consist of a high density, high Z material, such as an inorganic crystal or glass, which provides a high conversion efficiency for an incident photon. Table 1 lists some of the commonly used inorganic scintillators. The inorganic scintillators have the highest light output and provide the best energy resolution at lower energies. The last column of Table 1 gives the light output relative to NaI, which yields 38 000 optical photons per MeV of energy deposited (see Table 2). The incident photon undergoes an initial interaction on a high Z atom according to the processes described above, and the resulting electron or positron produces ionization which leads to the formation of electron-ion pairs. The electrons and ions then transfer their energy to luminescent centers in the material, which can be either intrinsic, such as in a BaF_2 crystal, or to a dopant or fluor which has been added as an activator, such as thallium (Tl) in the case NaI or CsI. The excited luminescent centers then radiate their energy in the form of scintillation light, typically either in the visible or UV wavelength range. In this process, each step takes place with a certain efficiency which contributes to the overall scintillation efficiency of the material. If we denote the conversion efficiency as β, the efficiency for energy transfer to the luminescent center as

S, and the radiative decay efficiency as Q, then the overall scintillation efficiency η is given by $\eta = \beta \cdot S \cdot Q$. Table 2 gives the respective efficiency factors for some commonly used scintillating crystals taken from Lempicki *et al.*(1993).

The Cherenkov materials, some of which are also listed in Table 1, produce light only by Cherenkov radiation and generally have a much lower light output than inorganic scintillators. Cerenkov radiation is the light emitted by charged particles when their velocity exceeds the phase velocity of light in the medium. It is a very small fraction of the total energy loss process. These materials are therefore used most often at higher energies where the total amount of energy deposited is much higher. The columns labeled Emission maximum and Decay time in Table 1 are not relevant for the Cherenkov materials. The emission is non-resonant and prompt so entries have been made with a $\check{C}$ to identify these materials.

A schematic representation of a sampling detector is shown in Fig. 5. Typically the passive medium consists of some high density material, such as lead, which provides the high photon conversion efficiency, while a lower density material is used as the active medium. Because only a faction of the total energy is measured, a sampling detector generally has poorer energy resolution than a totally active detector, but can be built for a much lower cost due to the smaller quantity of active detector material required. It is therefore widely used for large area, high energy calorimeters.

3.2 Energy Measurement

There are several techniques which are used to measure the energy deposited in the active medium in both a totally active and a sampling detector. These are generally based on either the direct detection of the ionization charge, or by the detection of either scintillation or Cherenkov light produced in the active medium. Direct ionization can be detected in either gases, liquids or solids, and the use of these materials depends largely on the energy range of interest. Because of their low density, gases are rarely used in gamma ray detection, even in sampling calorimeters. Liquids, in particular noble liquids, are often used in sampling detectors because of their relatively high Z, and the ability to easily collect the ionization charge using readout electrodes inside the detector. A high voltage is applied across the gap formed by these electrodes, which causes the charge to drift across the gap where it is collected and measured using charge sensitive detectors. Table 3 lists some of the properties of noble liquids which have been used for gamma ray detection. All of these liquids operate at cryogenic temperatures and are typically cooled using liquid nitrogen. Because of its low cost, liquid argon has been the most extensively used in large area high energy physics applications, (D0 Collaboration, 1994) and (SLD Collaboration, 1984).

Plastic scintillator, again because of its low cost, is also widely used in large area calorimeters. Table 4 gives a list of some of the commonly used plastic scintillators along with some of their properties. The light output is given relative to Anthracene, an early material, now rarely used except as the standard for reporting light output. One aspect of sampling detectors which use scintillating plastic is the need to collect the light produced onto a readout device. This is generally accomplished through the use of light guides, or by allowing the scintillation light to excite another fluorescent material known as a wavelength shifter which carries the light to the photodetector. The wavelength shifting technique has been extensively used because of its ability to provide a wide variety of readout techniques. One such method is illustrated in Fig. 6 (PHENIX collaboration, 1993). In this example, the light from scintillation plates, which are interleaved between plates of lead, is used to excite wavelength shifting fibers which pass longitudinally through the detector. The fibers are then bundled together at the back and read out with photomultiplier tubes. This provides a convenient way of placing the readout devices at the back of the detector where they will not interfere with any of the incident particles.

Finally, sampling detectors using silicon as the active medium have also been built and provide good energy resolution because of the large amount of charged produced. However, because of the significant cost of high purity silicon, these detectors have only been used in rather limited, small area applications.

4 Factors Affecting Gamma-ray Calorimeter Response

The overall performance of a gamma ray detector can be basically characterized by its resolution. There are three main types of resolution which are important experimentally. These are energy resolution, position resolution and time resolution, and there are a number of factors which determine these properties in any calorimeter design.

4.1 Energy Resolution

The energy resolution of a calorimeter can be parameterized by the following expression:

$$\left(\frac{\Delta E}{E}\right)^2 = \left(\frac{a}{\sqrt{E_g}}\right)^2 + \left(\frac{b}{E_g}\right)^2 + c^2. \tag{6}$$

The first term is called the *statistical* term and contains contributions to the energy resolution due to statistical fluctuations. These can be fluctuations in the amount of primary ionization produced (e.g., the total number of ionizing tracks produced in the electromagnetic shower), or by the fluctuations in the number of observed particles (either photoelectrons or ion pairs). Usually, for a high energy shower, the number of ionizing tracks produced is large, hence the fluctuations are rather small ($\leq 0.5\%/\sqrt{E}$), and the fluctuations in the number of observed particles dominates (Amaldi, 1981). For a sampling detector, this includes a contribution from the so-called *sampling fluctuations*, which are due to the fact that only a fraction of the energy is being detected, and this fraction can vary from one shower to the next. For high-Z inactive radiators of critical energy E_c, radiation length X_0 and total length L_x, the sampling fluctuation contribution to the energy resolution (full width at half maximum of the resulting signal) for gamma rays of energy E_g can be approximated as (Amaldi, 1981),

$$\frac{\Delta E}{E} = 7.5\% \sqrt{\frac{L_x}{X_0} \frac{E_c[\mathrm{MeV}]}{E_g[\mathrm{GeV}]} \frac{1}{G(Z, \cos\theta)}}. \tag{7}$$

Here, $G(Z, \cos\theta)$ is a compilcated function of geometry, the Z of the radiator material and the angle θ which characterizes the mean angular spread of particles around the shower axis, but it is typically a number between 1.0 and 1.3. In a sampling calorimeter, these fluctuations generally make the largest contribution to the statistical term in the resolution.

The term with coefficient b contains contributions that are fixed in magnitude relative to the observed signal. This term is called the *noise term* and contains contributions from various sources of noise. These includes any electronic noise in the readout devices or their associated electronics, as well as any constant background noise. Since this term goes as 1/E, it is most important at lower energies, and is often negligible at higher energies.

The term with coefficient c reflects complex functions of the detector that are rather slowly varying with energy and are often approximated by a constant. The two most important are the degree of shower containment and the uniformity of response throughout the active volume. As the fraction of the shower energy escaping a detector volume increases with increasing gamma-ray energy, the fluctuations in this signal loss grow until a roughly constant plateau in resolution is reached (Dowell *et al.*, 1987). This contribution can be made small with sufficiently large detector volumes, although the associated costs increase sharply with energy.

Even for large totally active detectors, such as NaI(Tl), inhomogenities in the crystal can be a fundamental limitation to the ultimate energy resolution one can achieve. The inhomogenities limit the performance through the variation in light generation and collection for the same amount of energy deposited in different regions of the active volume. This is a significant limitation at moderate energies, for example the 20 MeV shower shown in Fig. 3, where the variations in the shower distributions are large. The effect is much smaller at high energies where each shower fills a large detector volume (see Fig. 4). Variations are governed by crystal impurities and defects, by deviations in the local concentrations of dopant, by the reflective properties of crystal surfaces, by solid angle effects and the placement of the light collection devices, and by non-uniformities in efficiency across the surfaces of the light collectors (Dowell *et al.*, 1990). Controlling, or even predicting, any one of these components is quite difficult. However, their combined effect can be studied with muons and unfolded with the techniques of Computer Aided Tomography (CAT, or μCAT here) (Dowell *et al.*, 1990).

High-energy muons produce only narrow well-defined ionization tracks that can completely penetrate even large detectors. Being weakly interacting, they do not undergo nuclear reactions and can be used to deposit a known amount of energy in every element of detector volume along their path. The response to many muons traversing well defined paths can be combined with Fourier reconstruction algorithms to produce three dimensional images of the non-uniformities in light generation and collection. As an example, a section of such a μCAT map – a two dimensional slice through a 24 cm diameter $\times$ 36 cm long NaI(Tl) crystal viewed at one end by seven 7 cm photomultiplier tubes – is shown in Fig. 7. The grey-scale image shows the shift in the net collected signal for a nominal muon energy deposition of 5 MeV per cm of track length in each cell. (It is interesting to note that a visual inspection of the interior of this crystal failed to reveal any trace of the complex patterns evident in this μCAT map.) These non-uniformity images can be combined with Monte Carlo simulations of energy deposition in electromagnetic showers to accurately predict the resolution for gamma rays of any energy (Dowell *et al.*, 1990). Using the μCAT scan of Fig. 7, the predicted resolution for that detector is shown as the solid line in Fig. 8 together with measured results. (For comparison, the dashed curve gives the expected behavior of a perfectly uniform detector.) Although the non-uniformities are complex and highly varying, the volume sampled by the gamma-ray showers (see Fig. 3) is large and the net effect is to produce a nearly constant increase in the resolution at high energy.

4.2 Position Resolution

The spatial resolution of the calorimeter is determined primarily by the density of the detector materials as well as its spatial segmentation. As mentioned above, the containment of a shower in the transverse direction is determined by the Molière radius. Therefore, the natural unit for transverse segmentation of a calorimeter is in cells of approximately one Molière radius square. However, the position resolution of the calorimeter will be significantly better than this, since the shower position can be determined from a fit using information from many cells which contain energy from the shower. This can be done as a simple energy weighted average given by

$$x_{measured} = \frac{\Sigma w_i x_i}{\Sigma w_i} \tag{8}$$

where w_i is the energy measured in the *i-th* calorimeter cell and x is the position of that cell for the coordinate being measured. However, more sophisticated techniques are often used where the weighting parameters depend logarithmically on the energy in order to better account for large transverse energy fluctuations (Awes, 1992).

4.3 Time Resolution

There are two main aspects of the time resolution of a gamma ray calorimeter. The first is the variation in the measured arrival time of an incident particle, and the second is the ability of the calorimeter to resolve two particles which are close together in time. The first aspect, called the *leading edge* time resolution, is most important in time of flight applications, where the calorimeter is used to measure the transit time of particles arriving from some external source. The principle factors contributing to this resolution are: 1) the variation in time in the generation of the detectable signal, which can be either optical photons from a scintillator, Cherenkov photons, or ionization charge, 2) the time variation in the propagation of that signal to the detector, and 3) the variation in time due to changes in the amplitude or shape of the electronic pulse from the readout system, including contributions from electronic noise. In most cases, the time variation in the production of the primary signal is small compared to the other effects, since the time scale involved for producing either optical photons or ion pairs is rather short (≤ 1 ns). The second effect, which is mainly due to light or charge collection, can be significant, especially in a large calorimeter. It is affected by the propagation time in the detection medium (see Table 1 for indices of refraction in optical materials and Table 3 for drift velocities in noble liquids), as well as the size of the detector. The third effect includes the time variation in the detector response and readout system due to differences in energy deposition. Since the observed energy is subject to statistical fluctuations, this effect can be dominant, particularly at low energies. In general, the larger the prompt signal from the detector and the faster the response time of the readout system, the better will be the time resolution. For optical detectors producing large signals and using fast readout devices, it is possible to achieve time resolutions in the range from a few tenths down to a few hundreths of a nanosecond. For charge collection devices, depending on the size of the signal, it is possible to obtain time resolutions on the order of a few nanoseconds.

The second aspect of a calorimeter's time resolution is its so-called *pulse pair* resolution, or resolving time. This is the ability of the calorimeter to resolve two particles closely spaced in time. The main factor determining this resolution is the width in time of the electronic readout pulse. This depends on the decay time of the active material (given in Tables 1, 3 and 4), the propagation time in the detector, and the response time of the readout system. For a fast device, this can be on the order of a few nanoseconds. For slower detectors, it is possible to resolve two particles close in time by analyzing the pulse shape of the measured signal and comparing it to the known response for a single particle. This technique can provide improved time separation, but may give poorer energy resolution for particles whose arrival times are within the duration of the output pulse.

5 Readout Devices

5.1 Optical Detectors

A variety of different readout devices can be used to detect the signal produced in a gamma ray detector, and which device is used depends strongly on the type of detector (either totally absorbing or sampling), as well as on the type of detector material used. For scintillating materials, the most commonly used readout device is the photomultiplier tube. This device, shown schematically in Fig. 9, consists of a photocathode which converts either UV or visible photons into electrons (or, more appropriately, photoelectrons), which are then amplified by a series of electron amplifiers called dynodes. The photoelectrons are produced with an efficiency, know as the quantum efficiency, which is typically around 15-20%. The photoelectrons are then accelerated in an applied electric field and impinge on the dynode, producing several outgoing electrons for each incident electron. This process is repeated many times in subsequent stages of the photomultiplier tube until the desired gain has been achieved and the resulting charge is collected on the anode electrode. Gains of $10^6 - 10^8$ can be readily obtained with modern photomultipler tubes, providing the possibility of detecting even single photoelectrons, and hence single incident photons. Photomultiplier tubes are therefore one of the most sensitive types of readout devices used for detecting scintillation light. In addition, they can be designed to have a fast response time ($\sim$ a few nanoseconds), and can therefore be used in fast timing applications. The disadvantages of photomultiplier tubes are that they require rather high voltage to operate (typically 1-2 kV), and that they do not work well inside a magnetic field.

Another type of optical detector is a light sensitive photodiode. These can be either a silicon photodiode, such as those used in photocell detectors, or a vacuum photodiode, which has a construction similar to that of a photomultiplier tube having only a photocathode and anode electrode. An inherent property of these devices is that they have no intrinsic gain, and therefore rely on the incident radiation to produce a sufficiently large signal to be measured directly. However, some devices, such as avalanche photodiodes, can achieve modest gains ($\sim$ 10-100) by an amplification process within the silicon detector itself, which greatly improve their sensitivity to low light levels. Unfortunately, present day avalanche photodiodes have rather small active areas (< 0.5 cm^2) which limit their use in many applications. Other types of vacuum devices, such as phototriodes or phototetrodes, are essentially low gain photomultiplier tubes which can have large photocathode areas and can be used in other applications where modest gain is required.

5.2 Readout Electronics

Readout devices which have either no gain, or low intrinsic gain, usually require the use of a low noise, charge sensitive amplifier to detect the signal. The same is true for the detection of the direct ionization charge produced in noble liquids, such as those used in sampling calorimeters. In these cases, the primary signal can be on the order of only a few thousand electrons, and it is generally required to amplify this signal to the level of 10^7 electrons or more in order to be used for digitization and readout. This can be achieved with modern electronics through the use of low noise amplifiers and and signal shaping techniques (Radeka, 1988). These amplifiers are used to integrate the primary charge produced in the detector and deliver a signal which has the proper pulse shape and timing characteristics for the readout system. It is also generally required to carry out this signal processing with a minimum amount of noise introduced by the electronics in order to maximize the signal to noise ratio. With a careful design, it is possible to achieve noise levels on the order of a few hundred electrons with signal shaping times on the order of a few microseconds, or a few thousand electrons with shaping times on the order of a few nanoseconds. However, the choice of the appropriate signal shaping time and noise considerations depend strongly on the specific experimental application.

List of Works Cited

Amaldi, U. (1981), Phys. Scr. **23**, 409-424.

Awes, T., Obenshain, F. E., Plasil, F., Saini, S., Sorensen, S. P., Young, G. R. (1992), Nucl. Inst. Meth. **A311**, 130-138.

Bethe, H. A., Ashkin, J. (1953), in E. Segrè (Ed.), **Experimental Nucl. Phys.**, Vol. 1, New York: Wiley, p. 166.

Brun, R., Carminati, F. (1993), CERN Program Library Long Writeup W5013.

D0 Collaboration (1994), Nucl. Instr. Meth. **A338**, 185-253.

Dowell, D. H., Ziegler, W. P., Sandorfi, A. M., Ziegler, B., Schoch, B. (1987), Nucl. Instr. Meth. **A254**, 570-577.

Dowell, D. H., Sandorfi, A. M., Baron, A. Q. R., Fineman, B. J., Kistner, O. C., Matone, G., Thorn, C. E., Sealock, R. M. (1990), Nucl. Instr. Meth. **A286**, 183-201.

Hurlbut, C. R. (1985), presented Am. Nucl. Soc. Winter Meeting, excerpted from the **Bicron Catalog**, Newbury, OH: Bicron, Inc.

Kleinknecht, K. (1982), Phys. Rep. **84**, 85-161.

Lempicki, A., Wojtowicz, A. J., Berman, E. (1993), Nucl. Instr. Meth. **A333**, 304-311.

Nelson, W. R., Hirayama, H., Rogers, D. W. O. (1985), SLAC Report No. 265, Stanford CA.

PHENIX Collaboration (1993), in W.L.Kehoe (Ed.), BNL Report No. 48922, Upton, NY.

Radeka, V. (1988), Ann. Rev. Nucl. Part. Sci. **38**, 217-277.

Scott, W.T. (1963), Rev. Mod. Phys. **35**, 231-313.

SLD Collaboration (1984), SLAC Report No. 273, Stanford CA.

Tsai, Y.-S. (1974), Rev. Mod. Phys. **46**, 815-851, Tsai, Y.-S. (1977), Rev. Mod. Phys. **49**, 421-423.

Further Reading

Fabjan, C. W., Ludlam, T. (1982), Ann. Rev. Nucl. Part. Sci. **32**, 335-389.

Gratta, G., Newman, H., Zhu, R. Y. (1994), Ann. Rev. Nucl. Part. Sci. **44**, 453-500.

Majewski, S., Zorn, C. (1992), in F. Sauli (Ed.), **Instrumentation in High Energy Physics**, Singapore: World Scientific, p. 157.

Tables

	Density (g/cm^3)	Refractive Index	Radiation length (cm)	Molière radius (cm)	Emission max (nm)	Decay time (ns)	Light output
NaI(Tl)	3.67	1.85	2.59	4.5	410	250	1.00
BGO	7.13	2.20	1.12	2.4	480	300	0.15
BaF_2 (fast)	4.89	1.56	2.05	3.4	220	0.7	0.05
(slow)					310	620	0.20
CsI(Tl)	4.53	1.80	1.85	3.8	565	1000	1.40
CsI (fast)	4.53	1.80	1.85	3.8	305	10,35	0.10
(slow)					480	1000	0.02
CeF_3	6.16	1.68	1.70	2.6	340	10,30	0.10
$PbWO_4$	8.28	2.16	0.90	2.2	500	2,15	0.01
PbF_2	7.77	1.82	0.93	2.2	$\check{C}$	$\check{C}$	3.0×10^{-3}
Pb Glass(SF5)	4.08	1.67	2.54	3.7	$\check{C}$	$\check{C}$	1.0×10^{-3}
H_2O	1.00	1.33	36.1	6.8	$\check{C}$	$\check{C}$	0.8×10^{-3}

Table 1: Properties of Crystal Scintillators and Cherenkov Materials

Scintillator	L(γ's/MeV)	β	S	Q	η
NaI(Tl)	38 000	0.88	0.59	1.00	0.52
CsI(Tl)	65 000	0.97	0.99	1.00	0.96
CsI(pure)	2 000	0.97	0.29	0.10-0.15	0.03
BGO	8 200	0.69	1.00	0.13	0.09
BaF_2(fast)	1 800	<0.82	>0.9	1.00	0.08
BaF_2(slow)	9 950	<0.72	>0.33	1.00	0.24
CeF_3	3 200	0.61	0.13	1.00	0.08

Table 2: Efficiency Factors for Crystal Scintillators

	Liquid Ar	Liquid Kr	Liquid Xe
Density (g/cm^3)	1.39	2.45	3.06
Radiation Length (cm)	14.3	4.76	2.77
Molière radius (cm)	7.3	4.7	4.1
dE/dx (MeV/cm)	2.11	3.45	3.89
Drift velocity (cm/μsec)	0.5	0.5	0.3
W-value (eV/ion pair)	23.6	20.5	15.6
Dielectric constant	1.51	1.66	1.95
Triple point (°K)	84	116	161

Table 3: Properties of Noble Liquids

Scintillator	Light Output (% Anthracene)	Decay Time (ns)	Wavelength of Emission Max (nm)	Attenuation Length (cm)	Application
BC 400	65	2.4	423	250	General purpose
BC 404	68	1.8	408	120	Fast counting
BC 408	64	2.1	425	380	Large area
BC 412	60	3.3	434	400	Large area
BC 418	67	1.4	391	100	Ultra fast timing
BC 428	50	12.0	490	330	Green emitting

Table 4: Properties of Bicron Plastic Scintillators (Hurlbut, 1985)

Figures

Figure 1: The linear attenuation coefficient of sodium iodide and its decomposition into the contributions from the three interaction processes as a function of gamma ray energy. The data comes from the EGS4 Monte Carlo computer program for electron-gamma cascade shower modeling (Nelson *et al.*, 1985).

Figure 2: Schematic representation of how an electron-gamma cascade shower develops. A high energy gamma ray enters from the left, produces a pair which in turn emit bremsstrahlung to make more gamma rays, and so on.

Figure 3: Average relative energy deposition from an electron-gamma cascade shower. Size of the box represents the amount of energy deposited in 1 cm cubes of NaI in that position, averaged over many showers. Maximum box size occurs at a level such that the saturated boxes contain 90% of the gamma ray energy. A 20 MeV gamma ray enters from the left in the left plot and a 20 GeV one in the right. The radiation length of NaI is 2.6 cm and the Molière radius is 4.5 cm (see Table 1).

Figure 4: Average number of 1 cm cubes of NaI which receive any energy deposition during an electron-gamma cascade shower as a function of shower energy. The error bars represent the variation in the number of cubes from shower to shower.

Figure 5: Schematic representation of a sampling calorimeter.

Figure 6: A sampling calorimeter with wavelength shifting (WLS) fiber optic readout.

Figure 7: μCAT scan of a NaI detector.

Figure 8: Measured resolution of a NaI detector at several energies, the μCAT predicted resolution (solid line) and the resolution of a perfectly uniform detector (dashed curve).

Figure 9: Schematic representation of a photomultiplier tube.

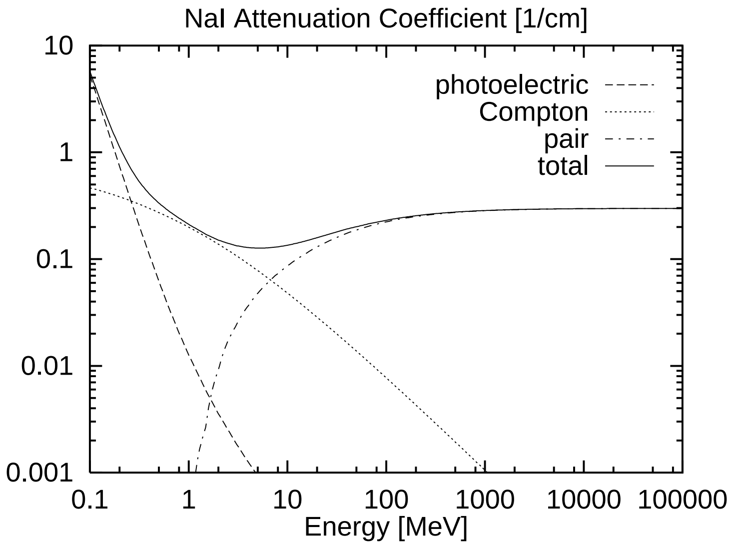

Figure 1:

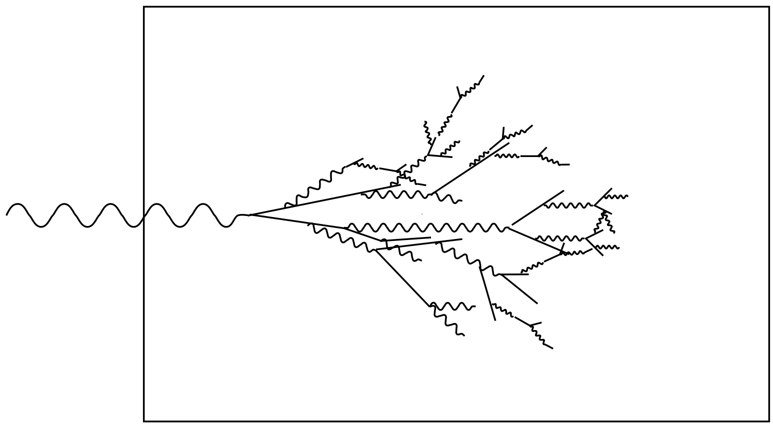

Figure 2:

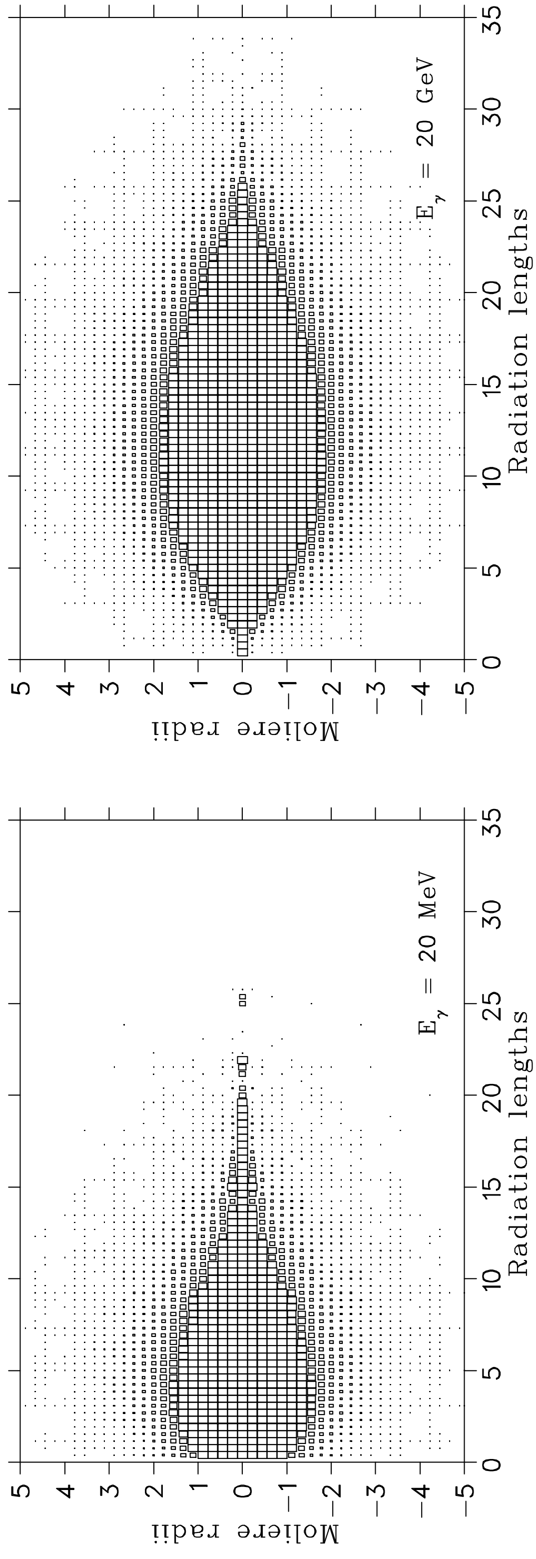

E$_\gamma$ = 20 MeV
E$_\gamma$ = 20 GeV
Radiation lengths
Moliere radii

Figure 3:

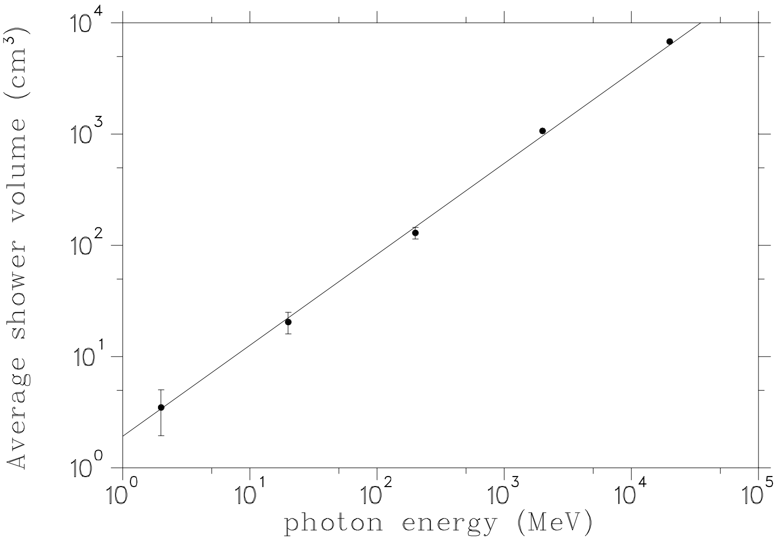

Figure 4:

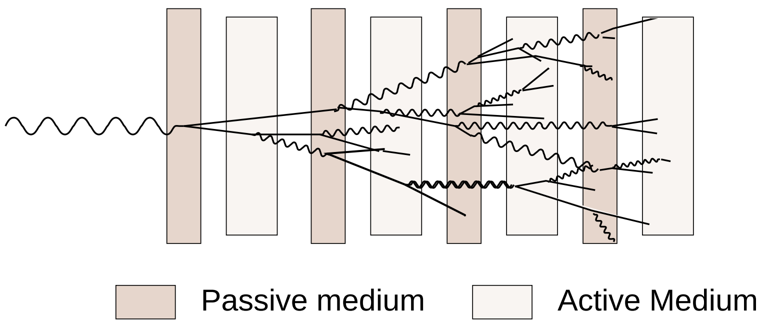

Figure 5:

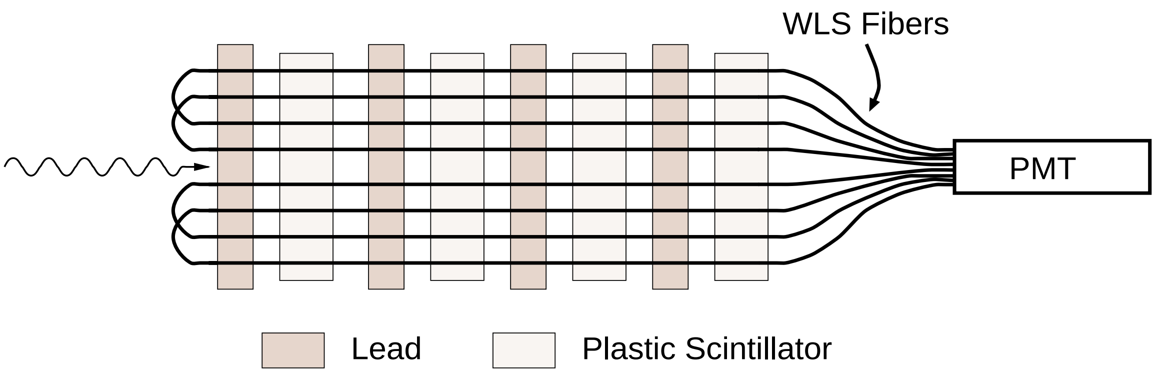

Figure 6:

Figure 7:

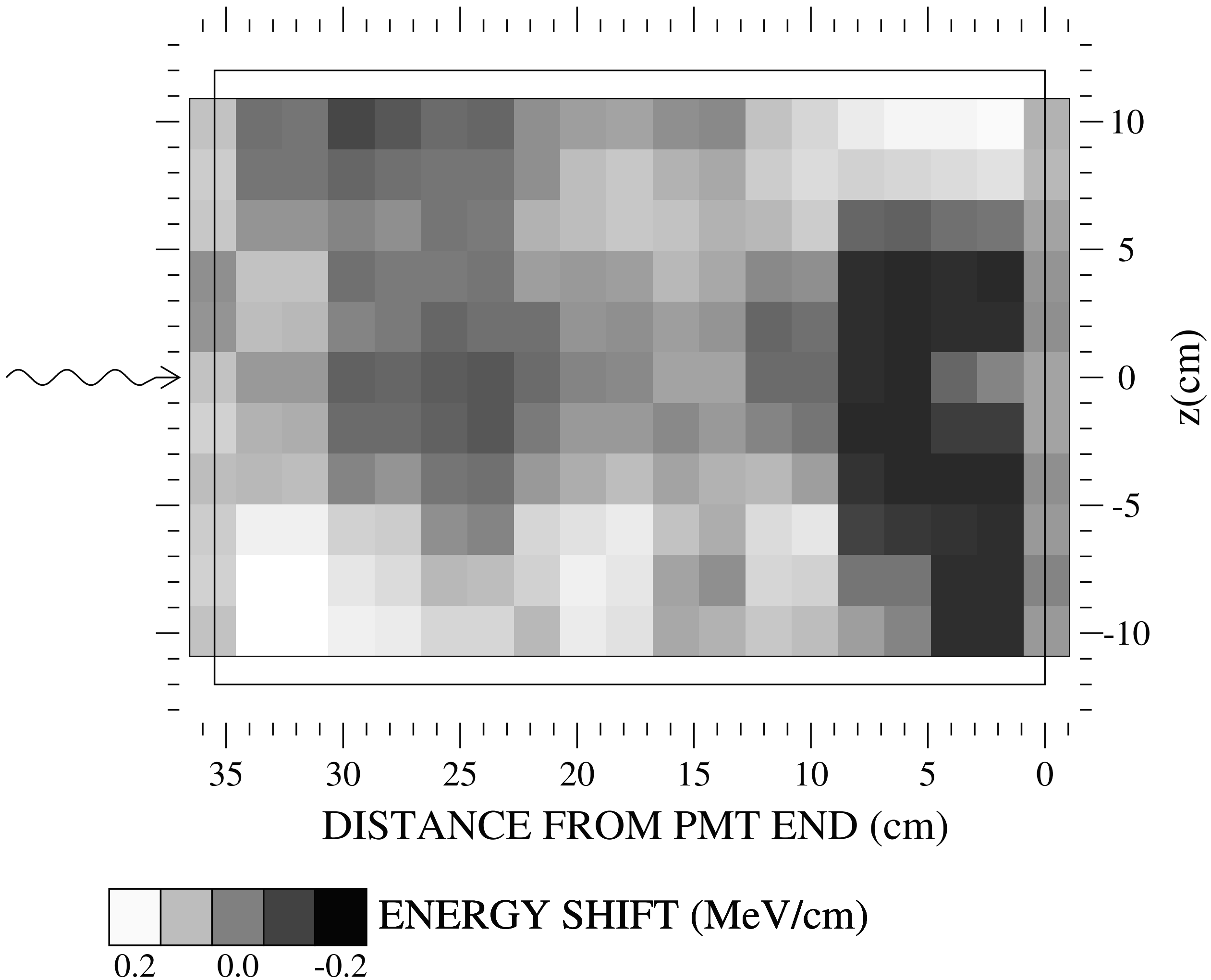
10
5
0
-5
-10
z(cm)
35 30 25 20 15 10 5 0
DISTANCE FROM PMT END (cm)
ENERGY SHIFT (MeV/cm)
0.2
0.0
-0.2

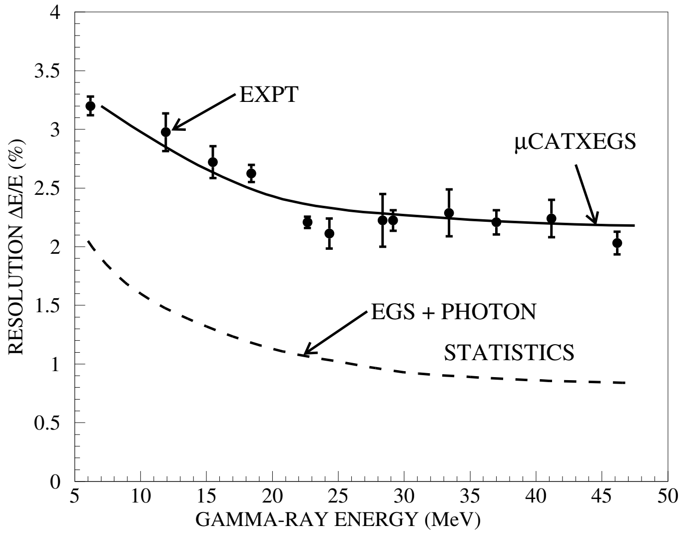

Figure 8:

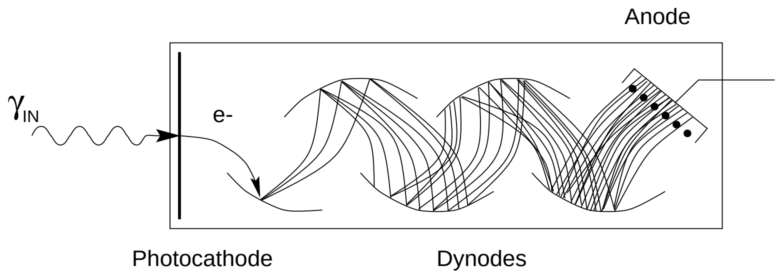

Figure 9: